ACS MATERIALS Au
AN OPEN ACCESS JOURNAL OF THE AMERICAN CHEMICAL SOCIETY

pubs.acs.org/materialsau

Article

Fabrication of 5D Fresnel Lenses via Additive Manufacturing

Murad Ali,* Fahad Alam, and Haider Butt*

Cite This: *ACS Mater. Au* 2022, 2, 602−613

Read Online

ACCESS | Metrics & More | Article Recommendations | Supporting Information

ABSTRACT: The consistent developments in additive manufacturing (AM) processes are revolutionizing the fabrication of 3-dimensional (3D) parts. Indeed, 3D printing processes are prompt, parallel, material efficient, and cost-effective, along with their capabilities to introduce added dimensions to the computer-aided design (CAD) models. Notably, 3D Printing is making progressive developments to fabricate optical devices such as regular lenses, contact lenses, waveguides, and more recently, Fresnel lenses. But extended functionalities of these optical devices are also desirable. Therefore, we demonstrate masked stereolithography (MSLA) based fabrication of five-dimensional (5D) Fresnel lenses by incorporating color-change phenomena (4th dimension) using thermochromic powder that changes color in response to external temperature variations (25−36 °C). The holographic diffraction effect (5th dimension) is produced by imprinting a diffraction grating during the printing process. Optical focusing performance for the 5D printed lenses has been evaluated by reporting achievable focal length, with <2 mm average deviation, without postprocessing in 450−650 nm spectral range. However, in the near IR region (850−980 nm), the average deviation was around 11.5 mm. Enhanced optical properties along with surface quality have been reported. Thus, MSLA process can fabricate optical components with promising applications in the fields of sensing and communication.

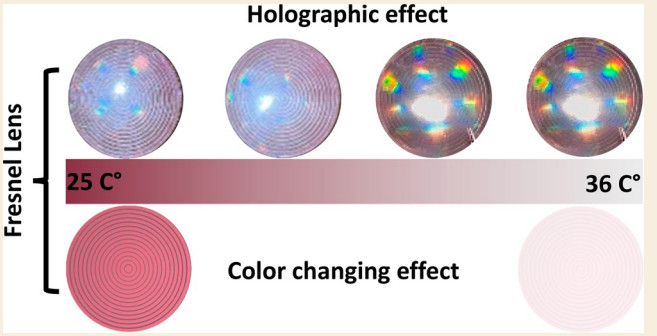

KEYWORDS: *Additive manufacturing, MSLA technology, 3D printing, Fresnel lens, Thermochromic powder, Diffraction grating, Holographic effect*

1. INTRODUCTION

In recent years, additive manufacturing (AM) or three-dimensional printing (3DP) has received much interest from the research community and industry. This approach is based on the layer-by-layer deposition of various materials, including polymers, metals, ceramics, and composite materials. 3D printing offers numerous advantages of being fast, flexible, and cost-effective. Moreover, benefits like low material waste, dimensional accuracy with a narrower tolerance range, and higher surface finish are reported in the literature. The design freedom is also highly regarded based on computer-aided design (CAD) to print 3D components. Therefore, 3D printing processes are more promising over conventional subtractive manufacturing processes such as turning, cutting, milling, ablation, etching, etc., due to more flexibility in design, shape complexity, material usage/wastage, and surface finish.[1,2] AM technologies comprise a variety of fabrication processes that can be categorized into seven macro-areas.[3] The various 3D printing processes include stereolithography, fused deposition modeling, digital light process, multijet fusion, direct metal laser sintering, electron beam melting, selective laser sintering, and polyjet. Based on their fundamental operating principles, each AM technology begins with a digital component model to be realized and then sliced into layers. In the layer-by-layer method, successive object layers are generated by curing liquid resins, extruding melted polymers and viscous solutions, fine sintering powders, or by laminating solid layers.[4]

Three-dimensional printing has proven its value by fabricating mechanical, electrical, and optical systems components. The 3D printed parts with improved mechanical, electrical, and thermal properties have multitude of applications in automotive, aerospace, construction, and medical fields. Recently, optical prototype fabrication via 3D printing has been the focus of a great deal of attention to achieve improved optical properties.[5,6] High-resolution printers have made it possible to print 3D micro- and nano-optical components to perform complex optical operations.[6,7] For instance, optical waveguides and lenses are immensely popular as light guiding devices, consisting of complex geometric shapes integrated with optical fibers, gas, and optofluidic sensors. The advances in additive manufacturing are pushing optical and photonic devices into new and unexplored architectures with immense commercialization potential.[7−12]

Received: March 14, 2022
Revised: May 9, 2022
Accepted: May 10, 2022
Published: May 31, 2022

https://doi.org/10.1021/acsmaterialsau.2c00026
ACS Mater. Au 2022, 2, 602−613

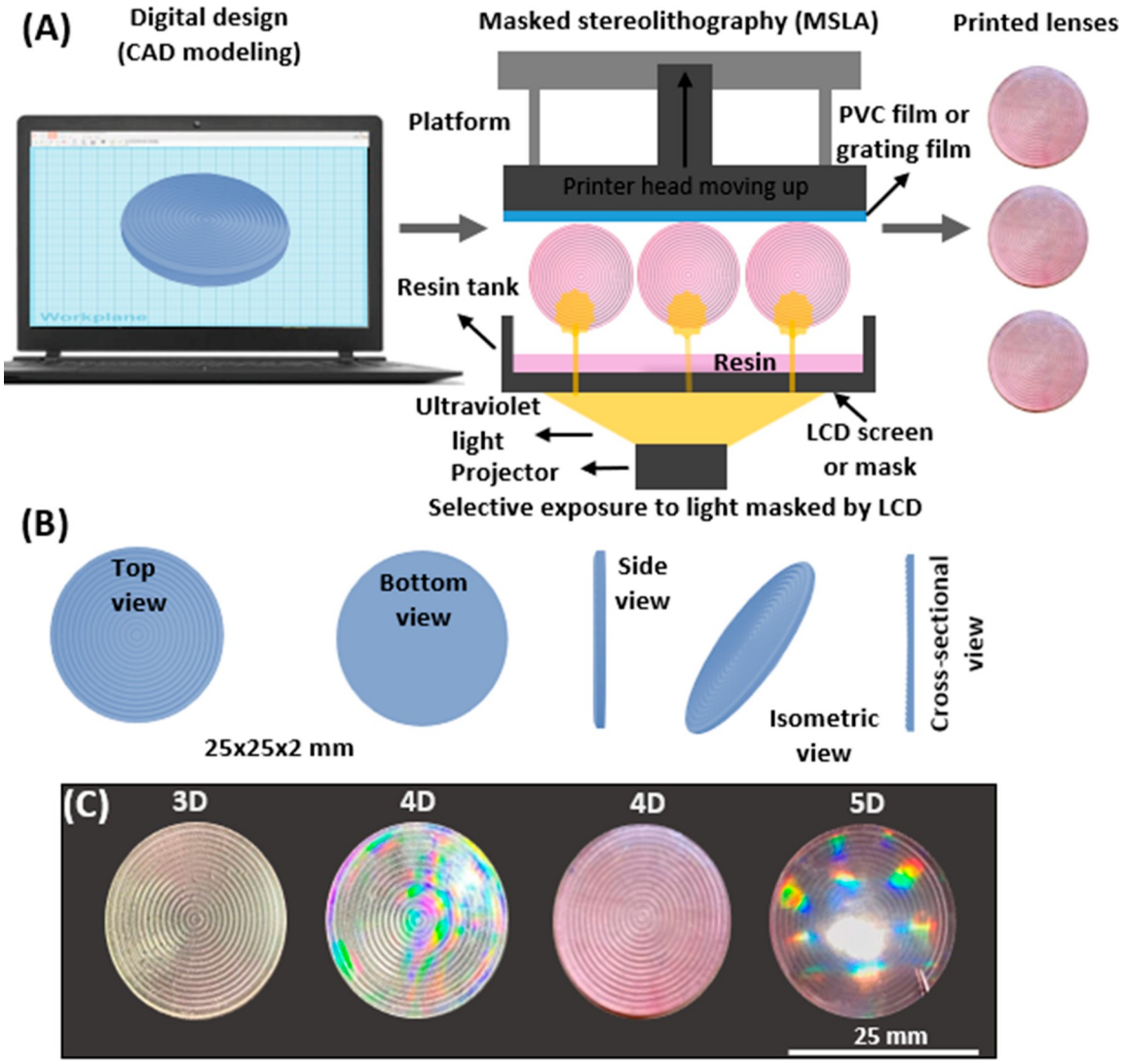

Figure 1. Overview of the 3D printing process, design, and final products. (A) Schematic illustration of MSLA-based 3D printing process. (B) Various views of Fresnel lens modeled in Solidworks. (C) Digital images of 3D (transparent), 4D (transparent and holographic), 4D (thermochromic), and 5D (thermochromic and holographic) Fresnel lenses in final form after a cleaning and drying process.

In optical designs, spherical and aspherical lenses form and guide light in various optical applications where the latter is more complex to manufacture because of having nonuniform surfaces.[13] Fresnel lenses are innovative spherical lenses characterized by optimized mass and materials. Fresnel lenses made of glass were widely used as collimators for lighthouses as soon as Augustin Jean Fresnel discovered their practical application in 1822. Such lenses were designed to resist the extremely high temperatures of the lighthouse environment as well as to be lighter and absorb less radiation than oil-covered mirrors. These lenses in the lighthouse are made of glass because of their lighter weight and low radiation absorption.[14−16] The significant role of such lenses is widely known from their utilization in condenser optics, field lenses, magnifiers, collimators, smartphones, miniature spectrometers, photovoltaic panels, ultrasonic devices, automobiles, and medical devices.[14,17−26]

Fresnel lenses are composed of concentric rings where each ring bends the light it captures to form a parallel beam of light. These lenses can be either imaging or nonimaging based on their intended uses. Fresnel lenses are most commonly manufactured by etching and layering of various optical materials. Poly(methyl methacrylate) (PMMA) exhibits excellent optical characteristics for multiple applications in solar technology especially in concentrating photovoltaic systems. Alternative silicon Fresnel lenses are also utilized in space applications such as solar concentrators with glass protection.[14,27] In addition, such lenses can also be manufactured by casting, injection molding, and compression molding. Unfortunately, these techniques use mold-based manufacturing processes with limited design and processing flexibility.[17,28,29] Therefore, 3D printing processes are more promising to explore the design strategies and complexity of Fresnel lenses. 3D printing also allows for multimaterials based lens production, for sensing and multifunctional optics. Consequently, we report five-dimensional (5D) Fresnel lenses based on 2-hydroxyethyl methacrylate (HEMA) resin, where the third and fourth dimensions come from their additional functionalities of thermal and holographic sensing introduced via masked stereolithography 3D printing.

https://doi.org/10.1021/acsmaterialsau.2c00026
ACS Mater. Au 2022, 2, 602−613

2. EXPERIMENTAL SECTION

2.1. Materials

The resin formulation included hydroxyethyl methacrylate (HEMA), polyethylene glycol diacrylate (PEGDA), and trimethylbenzoyl diphenylphosphine oxide (TPO) as the monomer, cross-linker, and photoinitiator, respectively. We mixed the monomer and cross-linker 1:1 ratio and added 2.5% of the photoinitiator to the resulting resin solution. The pink-colored thermochromic pigment powder purchased from Modern Stationery LLC Dubai was also added 0.08% wt % to resin material to change the optical properties of resin. The 3D printing was performed using transparent polyvinyl chloride (PVC) smooth plastic film (serving as support) on the print bed to achieve good surface quality. A Rainbow diffraction thin film (274 cm by 14.6 cm) provided by Rob's Store (Gurnee, IL) having 13 500-line grating was used for micropatterning of the surface. During printing, cleaning and drying were also accomplished using isopropyl alcohol (IPA), deionized (DI) water, and ethanol.

2.2. Design of Fresnel Lens and Printing Procedure

The Fresnel lens design includes the focal length calculations, number of concentric rings, and bending angle for each concentric ring forming a groove. Therefore, a Fresnel lens with a 25 mm diameter, 15 rings, and 2 mm thickness was designed, to give a 50 mm focal length. The rings had a constant width of 0.833 mm, and their heights increased radially outward to a maximum height of ∼0.4 mm for the last ring. The mathematical formulations for lens design are provided in Figure S1 (Supporting Information). The Fresnel lens was modeled in the computer-aided-design (CAD) software named Solidworks (Figure 1B). The designed details of the lens parameters are provided schematically (Figure S1, Supporting Information). The CAD file was transformed into a standard triangulation (STL) file. The STL file is then sliced for printing using the PrusaSlicer-2.2.0 slicer provided by the Original Prusa SL1 3D printer manufacturer.

The Prusa printer is based on MSLA technology which uses light pattern projection for the curing process. The MSLA technology provides better vertical and lateral resolutions along with fast curing of the whole layer exposed at once compared to stereolithography (SLA) technology. The schematic diagram of the MSLA printing process is illustrated in Figure 1A. In MSLA based printing process, light shines upward into a high-resolution LCD placed beneath the transparent resin tank. The LCD serves as a mask, allowing the printer to select the area in the resin bath to be cured. The maximum printing area was 5.9 by 4.7 by 2.6 in. with 25, 50, and 100 μm layer thicknesses. Our printing system can print features with 35, 50, and 100 μm thickness while lower layer thickness results in higher optical transmission of printed components. The complex optical structures such as photonic crystals are fabricated with layer thickness around 25 μm.[30] This study considered suitable printing parameters, such as 25 μm layer thickness, 40 s time exposure for the first layer, and 20 s for the remaining layers. The translucent orange hood protects the UV-sensitive resin from ambient UV light that could prematurely harden the resin material. The PVC film was applied to the print bed to avoid the usage of any support structures to be printed and to improve print surface quality. The printed lenses were washed with ethanol and dried at ambient conditions. After the washing and cleaning process, the resulting Fresnel lenses are shown in Figure 1C.

2.3. Material Characterization of Fresnel Lenses

The optical properties of the printed Fresnel lenses were measured using customized homemade optical setups. An optical microscope (AXIO, Scope 1, Germany) was used to measure the optical transmission spectra. Optical images of the lenses were captured digitally using a digital microscope with a magnification of 300× and an image sensor of 5 megapixels. The rainbow grating sheet was characterized by optical diffraction with three monochromatic light sources (blue, green, and red). Samples were positioned 220 mm from the plane white screen, which was used to record the diffraction patterns. Field emission gun scanning electron microscopy (FEG-SEM) was utilized to analyze the thin film with the holographic design and printed lenses (JEOL JSM-7610F). A 24 nm Pt-coating was deposited on the samples with a direct current sputtering machine (JEOL JEC-3000FC) to avoid charging during SEM imaging. The coating was performed at 40 mA current for 120 s in a vacuum of less than 5 Pa. Atomic force microscopy (AFM; Asylum Research, Santa Barbara, CA) was used to determine the surface roughness. X-ray diffraction patterns via a D2 PHASER diffractometer were recorded using Ni-filtered Cu Kα radiation (λ = 1.54284 Å) at 30 kV. Surface wettability was investigated using a homemade setup to measure the surface contact angles. The measurements were taken by the LBADSA method[31] and were repeated five times to account for standard deviation errors by using a sessile drop of 10 μL.

2.4. Focal Length Measurement

Focal length measurements were done to evaluate the focusing performance of the printed lenses. For this purpose, three monochromatic light sources of different wavelengths have been used to illuminate the lenses. A homemade setup was designed for the focal length measurements (Figure 5). The experimental setup comprised of light sources (450, 532, 650, 850, and 980 nm laser diodes covering from the ultraviolet (UV) to infrared (IR) spectral range (450−980 nm)), a beam expander, lens mounting platform with flexible arms and adjustable height, and optical power meter. The light source produces a monochromatic beam of light, the beam expander spreads the light over the entire surface of lens, and the power meter records the transmitted light intensity through lenses. These components are precisely aligned with the help of kinematics mounts on an optical bench to guarantee the propagation of a collimated light beam going through the lens and converging at the focusing point. The maximum power intensity (W/m^2) was found at the focusing point by varying the translational positions of the power meter on the optical bench. The recorded power intensity values were normalized with the experimentally measured power of each laser source. Before the beam expander, the power intensity of all laser sources was measured for normalization.

2.5. 5D Fresnel Lenses (Holography and Temperature Sensing)

Thermochromic materials undergo a coloration or discoloration process at specific temperatures known as thermochromic transition temperatures. When the temperature reaches a particular value, the color change occurs rapidly. Here, thermochromic pigment powder was added as a responsive material to the transparent hydrogel resin. Indeed, such a powder can reversibly change the color as a function of surface temperature, enabling temperature sensing which we present as the fourth dimension (4D) of the printed device. Thermochromic pigment powders are colorless at higher temperatures while being colored at low temperatures[32,33] A thermochromic pigment powder (pink) of 0.08 vol % concentration was mixed with liquid monomer resin and magnetically stirred for 15 min (Figure S2, Supporting Information). The prepared mixtures with 0.08 vol % pink-colored pigment powders have the most negligible impact on the lens transmission. Various concentrations (low or high) of pigment powder could be used for parameter-specific optical applications. The mixed solutions were transferred separately to resin vat for printing (Figure S2). After successful printing, 4D Fresnel lens samples were washed with isopropyl alcohol and dried, as discussed earlier. The fifth dimension was introduced to the 4D printed lenses by embedding microscale holographic patterns on one side of the lenses, leading to 5D printing. The holographic film was applied to print bed of the 3D printer to imprint the holographic micropattern onto the first printed layer for producing 5D printed Fresnel lenses. A variety of textured surfaces with holographic effects can be embedded into 3D parts. Here, we report a microsize holographic pattern embedded in Fresnel lens that enables the lens to focus light and simultaneously exhibits the holographic effect.

Therefore, another optical setup to investigate the thermochromic behavior of the 5D fabricated lenses was designed. It is challenging to heat lenses uniformly for color intensity variation with temperature. Therefore, the lens was immersed in deionized water and the temperature was gradually increased from 25 to 36 °C with 1 °C step

https://doi.org/10.1021/acsmaterialsau.2c00026
ACS Mater. Au 2022, 2, 602−613

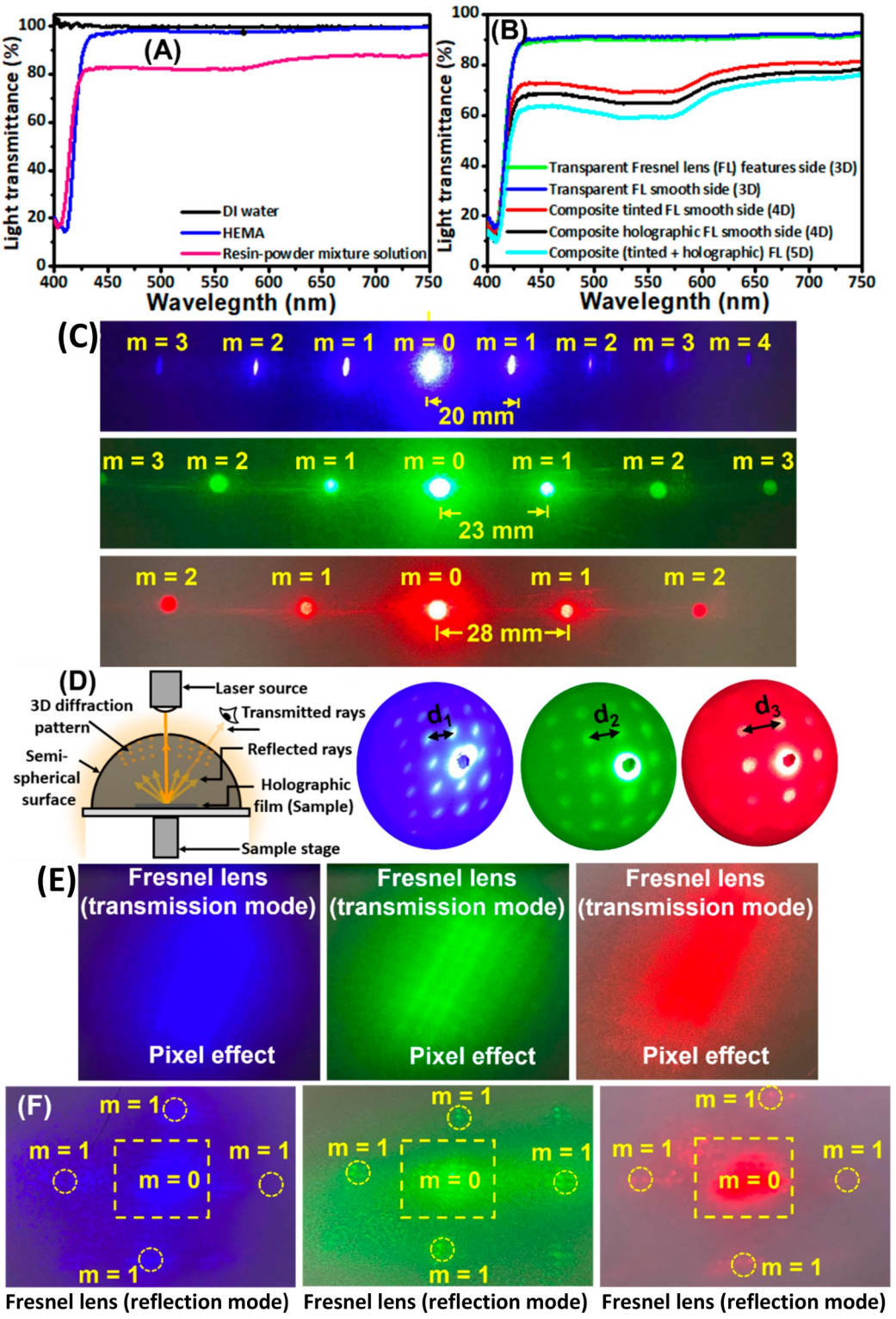

Figure 2. Optical characterization of liquid resin, printed samples, thin holographic film, and 5D printed Fresnel lenses in transmission and reflectance modes. (A,B) Optical transmission spectra of the hydrogel resin before and after printing. (C,D) Diffraction analysis of thin grating film with three laser sources (450, 532, and 650 nm) and 3D representation of the diffraction patterns. (E) Optical pixel effect of 5D printed lenses with three laser sources in transmission mode. (F) Diffraction pattern of the 5D printed lenses in reflection mode.

increase. The lens response based on coloration was stable despite the lens material being based on a HEMA hydrogel. The water content absorption varies the refractive index, as water is a low refractive index material.[34] Here, refractive index variations are not considered for the sole purpose of the experiment to homogeneously heat the fabricated lenses.

3. RESULTS AND DISCUSSION

MSLA-based 3D printing has shown promising results by fabricating the current lens design with the desired geometrical parameters and dimensions. The process is even capable of other complex shapes with close tolerances depending on printer

https://doi.org/10.1021/acsmaterialsau.2c00026
ACS Mater. Au 2022, 2, 602−613

capabilities. The chosen lens materials exhibited suitable optical properties for light focusing and thermal sensing without any adverse effects. The optical transmission spectra for lens materials were recorded before and after the printing process Figure 2A,B. The transmittance measurement setup was composed of an Ocean Optics spectrometer (USB 4000) connected to an optical microscope equipped with a white light source for transmittance measurement. A collimated beam of white light passes through the sample and is then collected by a high numerical aperture microscope objective. The collected light was directed into a spectrometer through a multimode optical fiber. The transmission measurements were conducted with DI water as a reference with an average transmittance value of 99.92%.

The prepared HEMA resin transmits all the wavelengths but with a slightly lower average transmission value (∼94%) than that of DI water. The resin transmittance above 450 nm wavelength was close to 98%. Thus, the prepared UV curable resin suitably fabricates optical devices such as Fresnel lenses. However, the addition of pigment powder resulted in lower transmittance due to light absorption and scattering caused by the powder particles. Therefore, the average transmittance value was reduced for the resin-powder mixture solution to ∼82%. A slight dip in transmission spectrum around the 500−575 wavelength range refers to the absorption range of the pigment. However, beyond 600 nm wavelength the transmittance increased to the maximum value of ∼84% (Figure 2A). Optical transmission measurements for the printed samples after the curing process are shown in Figure 2B. The transmission varied slightly depending on the side (featureless flat side or side with rings) from which the light propagated into the lens first. The transmission was higher when the light entered from the flat side as the light beam was more uniform and with no diffraction while propagating through the lens. The transparent Fresnel lenses exhibited the highest average transmittance values of near 86.8% and 91.4% for sides with rings (features) and without rings (features and smooth sides), respectively. Compared to the transparent liquid resin before printing, 3D printed samples resulted in lower transmittance (∼10% average reduction) upon curing (3D printed), probably due to strong bonding in solid materials offering more resistance to light propagation through the material.[35] Also, printed samples had multiple layers which function as scattering interfaces for the light propagating through the lens media. The addition of pigment powder resulted in coloration (pink) and reduced the transmission as expected. The addition of powder or nanoparticles to clear resin encourages the wavelength selective absorption and scattering of the incoming light rays. However, optimum powder concentration (0.08%) avoided significant reduction in light transmission, recording a 72.29% average value. Light transmission through composite materials varies according to their absorption and scattering properties,[36] and both depend on the particle size distribution and the mismatch between the refractive indices between particles and the resin matrix.[37] Moreover, light transmission through the lens could be controlled using various pigment powder concentrations depending on specific requirements. Interestingly, powder addition leads to the selective wavelength filtering capability of Fresnel lenses at room temperature.[38,39] Furthermore, tinted and holographic lenses (4D) responded similarly to transmission spectra with tiny deviations. Compared to all samples, 5D lenses exhibit the lowest transmission (64.05%) due to the holographic micropattern (caused light diffraction) and powder addition (caused light absorption/scattering) but could be improved by methods mentioned earlier.

The diffraction analysis of grating film was done using blue (450 nm), green (532 nm), and red (650 nm) lasers, revealing various diffraction orders upon illumination (Figure 2C). According to the grating equation ($\Lambda = m\lambda/\sin\theta$, where m is diffraction order, λ is the incident light wavelength, and θ is diffraction angle), the spacing between two diffraction orders or grating period Λ decreases as the light wavelength shortens.[40] Thus, for the blue and red light, the minimum and maximum grating distances observed are 20 and 28 mm, respectively. Similarly, by shortening the wavelength (from red to blue), diffraction angles exhibited a reducing trend for red (15.07°, 7.47°, 0°), green (12.28°, 6.10°, 0°), and blue (10.37°, 5.16°, 0°) lasers for the first three diffraction orders (m = 0, ±1, ±2), respectively.[41] A translucent hemispherical surface was used to view the 3D diffraction patterns produced in response to the normally incident laser beams, and a similar trend of the reducing diffracted angles ($d_3 > d_2 > d_1$) was observed with incident light wavelength decreasing from red to blue (Figure 2D). The 5D lens was exposed to a collimated high-intensity laser beam in transmission and reflection modes (Figure 2E,F). Interestingly, when light passes through volume of printed material in transmission mode, the holographic effect diminishes. However, the pixel effect (from the 3D printers display) could be observed due to the finite pixels size used in the printing process (Figure 2E). The diffraction effect (from the imprinted grating) could be observed by reversing the light direction and illuminating reflection mode Therefore, the lens was placed at 45° to laser light sources, and diffraction patterns for blue, green, and red lasers were recorded in reflection mode. The most prominent diffraction orders are 0 and +1 in reflection mode (Figure 2F).

Surface topography using SEM micrographs to present the entire lens with 15 rings (from a set of combined images) is reported in Figure 3. MSLA-based 3D printing uses the mask to illuminate pixels during printing specific areas. Here, the effect of the pixels can be seen clearly without surface defects confirming process integrity (Figure 3A). The color changing pigment powder was characterized using SEM micrograph that revealed spherical morphology and comprised of agglomerates (Figure 3B). The thin holographic film exhibits rhombohedral morphology, imprinted from the grating thin film, with features size of around 5 μm (Figure 3C). Rhombohedral features were successfully embedded on the lens surface using the current printing process Figure 3D. Although all the efforts were made to print a completely homogeneous pattern, but small discrepancies are possible in the physical processes. The homogeneity of the pattern is possibly affected by these three main factors: (1) slight misalignment of the holographic sheet on the print bed, (2) high cure time of the first layer, and (3) applying inadequate force during pattern removal from the print bed. The holographic effect from these features in response to white light surface can be observed clearly in Figure 1C. Lens samples were fractured for SEM characterization to examine the binding quality of powders and resin matrix upon photopolymerization. The embedded powder particles are encircled on the fractured surface, and the presence of no voids justifies complete layers diffusion during the printing process Figure 3E. Also, fracturing led to particle pull-out represented by dotted circles are shown in Figure 3F.

Optical polarization spectroscopy analysis was performed to record optical transmission spectra for the lens samples; the

https://doi.org/10.1021/acsmaterialsau.2c00026
ACS Mater. Au 2022, 2, 602−613

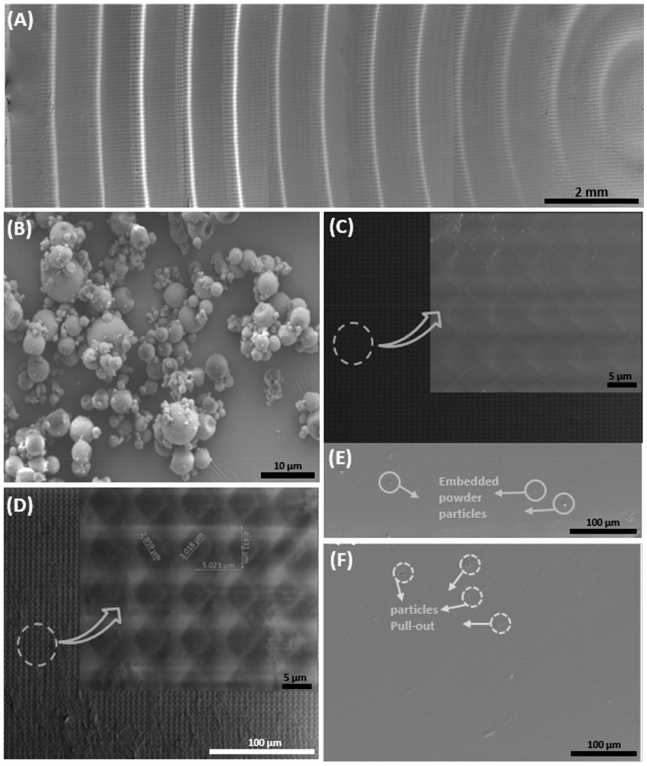

Figure 3. Scanning electron microscopy (SEM) micrographs of the printed lens. (A) Surface topography of the printed lens with 15 rings. (B) Morphology of thermionic pigment powder used for coloration. (C) Surface topography of micropatterned thin grating film. (D) Surface details of microfeatures imprinted on the lens surface. (E) Quality of fractured lens surface after printing with embedded powder particles. (F) Surface quality of after printed lens after fracture indicating particle pull-out.

transmission spectra for all the lenses were obtained from 0° to 90° polarization angles with 10° step size, as presented in Figure 4. The experimental setup consists of the light source, polarizer, and analyzer as integral components for examining polarization dependent transmission (Figure 4A). Polarized light passes through the sample and then from the analyzer to confirm any shift in optical polarization of light due to resin crystallization, as shown in Figure 4B. The light polarization through all the lenses is angle-dependent polarization. The polarization angle is zero when the axes of the polarizer and analyzer are parallel, allowing maximum light to pass through and exhibiting maximum transmission spectra (highest transmission intensity), as shown in Figure 4C−F. According to Malus' law, transmission spectra intensities are reduced when the polarization angle increases from 0° to 90°. Upon reaching the 90° polarization angle, the axes of the polarizer and analyzer are crossed, leading to complete blockage of incident light.[42] The reduction in intensities of full transmission spectra for all the lenses is evident (Figure 4C−F). Thus, all the lenses (3D, 4D, and 5D) responded similarly to polarized light and indicated that lenses do not influence light polarization. The results further confirm that transparent, tinted, holographic, and their hybrid (tinted holographic) lenses do not exhibit polarization depending optical properties since there is no correlation between the degree of tinting and holographic effect with the intensity of polarized light transmission. The polarization-based measurements allow us to depict that no crystallization has occurred and the printed composite sample is not birefringent. Moreover, the findings suggest that MSLA-based 3D printing is a viable option for producing transparent (3D), tinted (4D), holographic (4D), and tinted plus holographic (5D) Fresnel lenses (Figure 4C−F).

The focusing performance of lenses was evaluated by focal length measurements using a homemade optical setup (Figure 5A). All the lenses were illuminated with five lasers from the UV to IR (450−980 nm) spectral range for measuring the focal points. Each figure is represented by five curves using different symbols for focal length measurements. A blank symbol represents the focal point in each curve. The focal lengths for the transparent lens (3D) in response to 450, 532, and 650 nm lasers were 58.5, 58.5, and 64.5 mm, respectively (Figure 5B). Notably, measured focal lengths were obtained with 10.5 mm average deviations from the designed value (50 mm) without postprocessing. However, the deviation was slightly more for the red laser (less than 15 mm) due to wavelength dependent focusing nature of lenses. Moreover, for 850 and 980 nm lasers (near IR wavelengths), focal lengths were recorded as 55.5 and 52.5 mm, respectively, with a 4 mm average deviation from the designed value. The results confirm that MSLA-based 3D printing is suitable for fabricating Fresnel lenses and similar optical components. The focal lengths for all the lenses were determined using the same procedure.

The focal lengths for composite tinted Fresnel lens (4D) were 38, 43, and 49 mm for the 450, 532, and 650 nm lasers. Again, the results are promising for tinted lenses with an average deviation of 7 mm from the UV to visible spectral range (Figure 5C). However, near IR wavelengths resulted in 70.5 and 67.5 mm focal lengths for 850 and 980 nm lasers with larger deviations from the designed values. The significant average focal length variations (13.5 mm) might be due to variations in signal strength, misalignment, or surface roughness. The tinted thermochromic lenses are also useful for wavelength selective color filtering applications. Composite holographic lens (4D) behaved similarly with 37, 43, and 52 mm focal lengths for the 450, 532, and 650 nm lasers, respectively, with an average deviation of about 7 mm (Figure 5D). The lens recorded focal lengths of 58.5 and 61.5 mm using 850 and 980 nm lasers, respectively, with 10 mm average deviation. An average improvement of 3.5 mm in focal length was achieved when using near IR wavelengths for composite holographic Fresnel lens compared to tinted Fresnel lens.

Eventually, the composite (tinted and holographic) Fresnel lens (5D) was assessed for focal length measurements. The 5D lens remarkably performed well and generated focal points at 47, 49, and 49 mm for 450, 532, and 650 nm lasers, respectively, with less than 2 mm average deviation (Figure 5D). For the 850 and 980 nm lasers, the same focal length of 61.5 mm was obtained from the 5D lens. The focal length average deviation for 5D Fresnel was between the tinted Fresnel lens (4D) and the holographic Fresnel lens (4D) using near IR lasers. All the lenses performed focusing with experimental results in agreement with the designed parameters; the 5D lens exhibited significant performance as a light-guiding optical device. These promising results consolidated the idea that our current approach can be used to fabricate 4D and 5D hierarchical optical devices for photonic and sensing applications. The focal length measurements were carried out at room temperature. It is proven that temperature affects the focal length of the optical systems.[43] With the increase in temperature, the wavelength range transmitting through the Fresnel lens increases allowing all the light to pass through affecting the filtering wavelengths. Thus,

https://doi.org/10.1021/acsmaterialsau.2c00026
ACS Mater. Au 2022, 2, 602−613

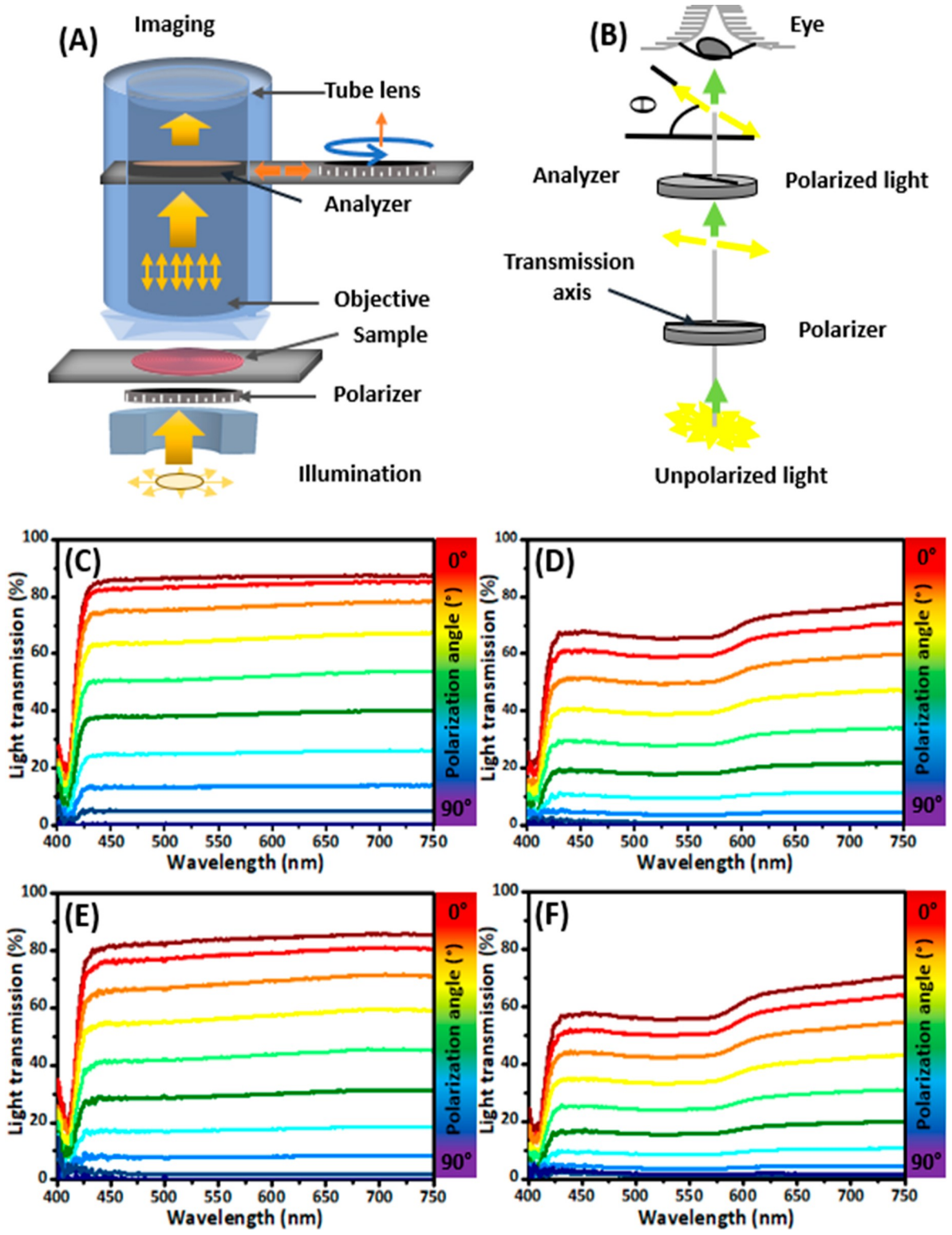

Figure 4. Optical polarization analysis of printed samples. (A) Schematic illustration of polarization setup for transmission based spectroscopic analysis. (B) Schematic illustration of light polarization process. Angular dependent optical transmission spectra of Fresnel lenses: (C) transparent lens (3D), (D) composite tinted lens (4D), (E) composite holographic lens (4D), and (F) composite (tinted + holographic) lens (5D).

high temperature influences the filtering wavelength in the case of color Fresnel lenses.

Recently, significant improvements have been reported in the design and applications of 3D printed lenses.[39,44] Therefore, adding extra functionalities to such lenses is always desirable to extend their utilization in optical systems. The color-changing characteristics in 4D and 5D lenses were imparted by the addition of a thermionic pigment powder into the resin matrix, which allows lenses to change colors reversibly upon cooling and heating (Figure 6A,B). The 5D lens exhibits color changes from pink to transparent with a 1 °C step increase in temperature from 25 to 36 °C upon heating (Figure 6A). The same color-

https://doi.org/10.1021/acsmaterialsau.2c00026
ACS Mater. Au 2022, 2, 602−613

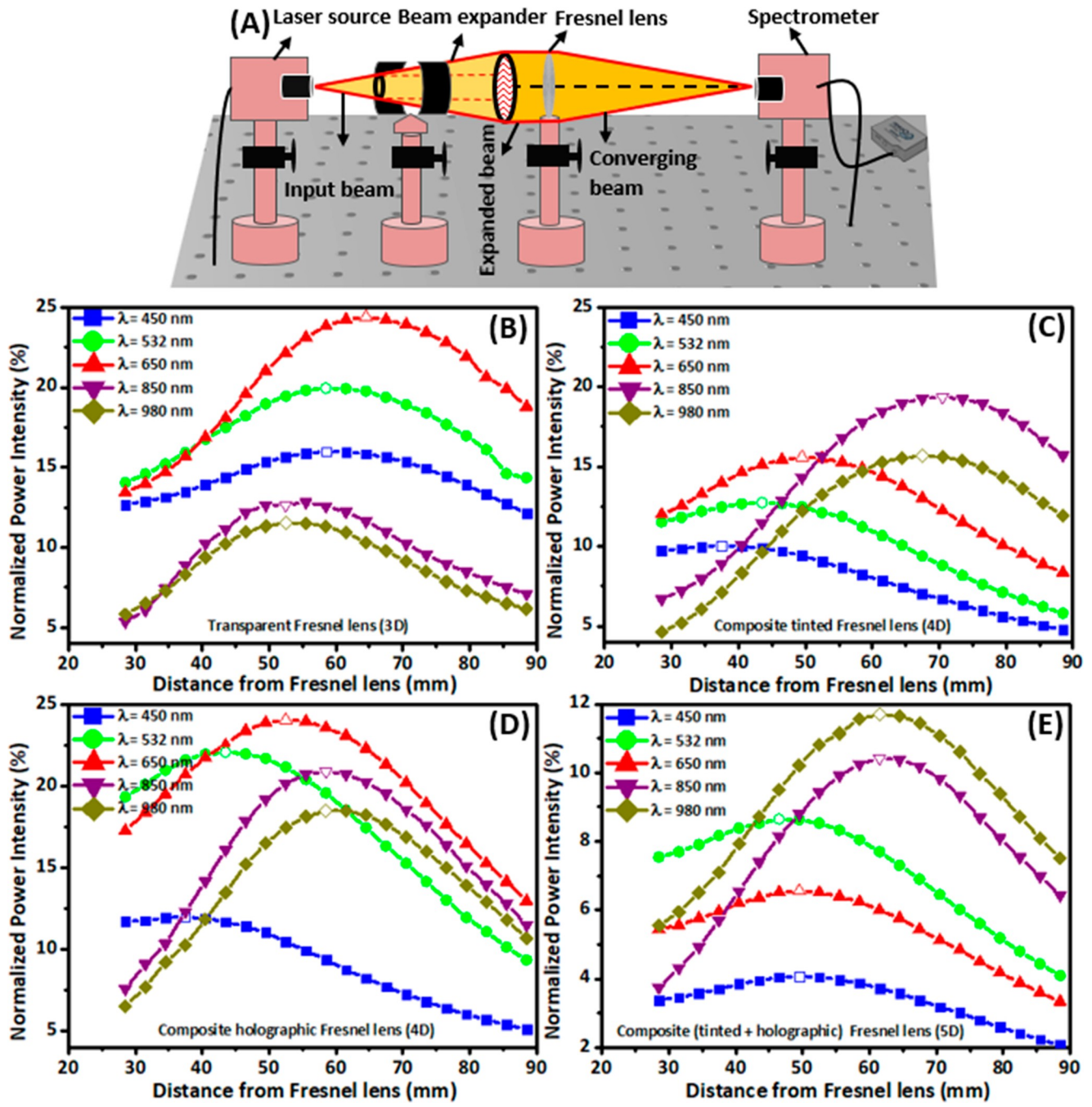

Figure 5. Optical performance evaluation of Fresnel lenses by focal length measurements with five laser sources. (A) Schematic illustration of experimental setup for focal length measurements. Focal length measurements for (B) transparent lens (3D), (C) composite tinted lens (4D), (D) composite holographic lens (4D), and (E) composite (tinted + holographic) lens (5D).

changing response was observed upon cooling the lens from 36 to 25 °C (Figure 6B). Analyzing the digital image requires extracting color information from the pixels of the color sample chart in terms of red (R), green (G), and blue (B) codes.[45] Pixels are the points that make up a digital image. The pixels are composed of three components, red, green, and blue.[46] Researchers have also used the red, green, blue-distance (RGB-D) method with the Kinect 3D sensor for tracking purposes.[47,48] A line through the diameter of the 5D lens at specific temperatures (25, 27, 29, 33, and 36 °C) was drawn, and RGB codes were extracted to analyze each component with increasing temperature (Figure 6C). The red, blue, and green spectra represent the R, G, and B components of the digital image analyzed. The pink color is evident from the first image at 25 °C, where the R-component spectrum has the average highest intensity (~198) while B and R components stayed at an average intensity value of ~155. When the temperature increases, the intensity of the R-component declines and reaches ~194 at 36 °C. Interestingly, the separation between B and G components increases gradually with the temperature rise. The average difference in their intensities at 25 and 36 °C obtained was 0.27 (lowest) and 15.57 (highest). These results confirm the color change response of the 5D lens with temperature as an external stimulus. These results also suggest that the current

https://doi.org/10.1021/acsmaterialsau.2c00026
ACS Mater. Au 2022, 2, 602−613

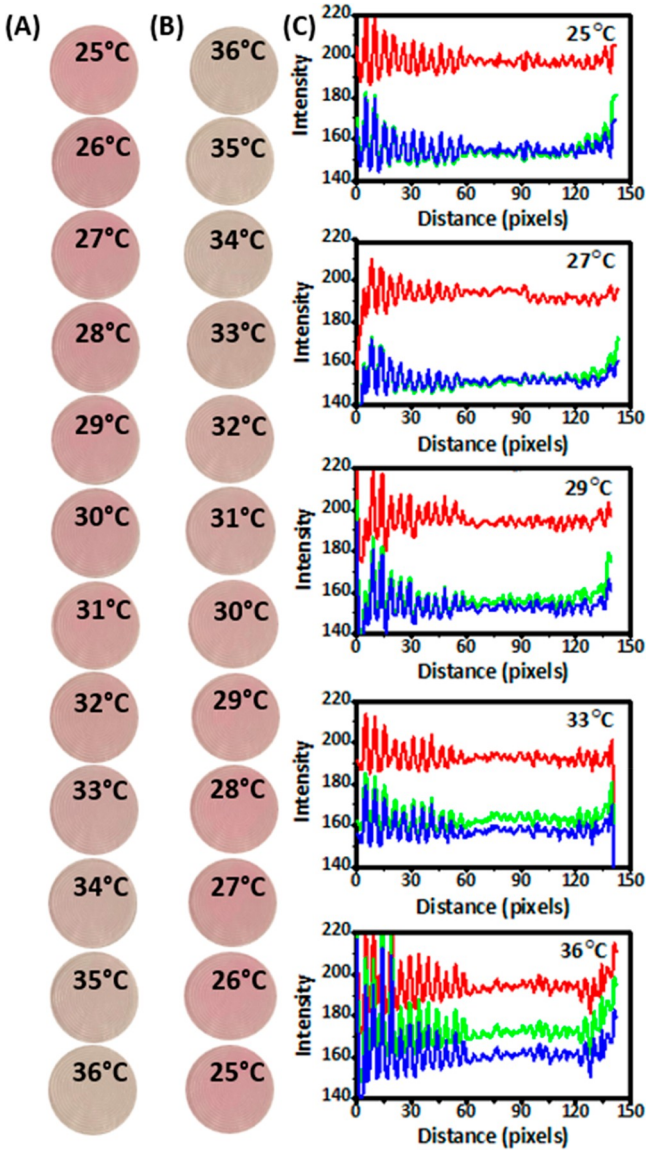

Figure 6. Temperature sensing analysis of 5D Fresnel lens in the 25 °C (complete coloration) to 36 °C (complete discoloration) temperature range. (A) Discoloration of lens by increasing temperature from 25 to 36 °C (heating cycle). (B) Coloration of lens by decreasing the temperature from 36 to 25 °C (cooling cycle). (C) RGB code based spectra for selected temperatures (between 25 and 36 °C exhibiting the color intensity variation phenomenon.

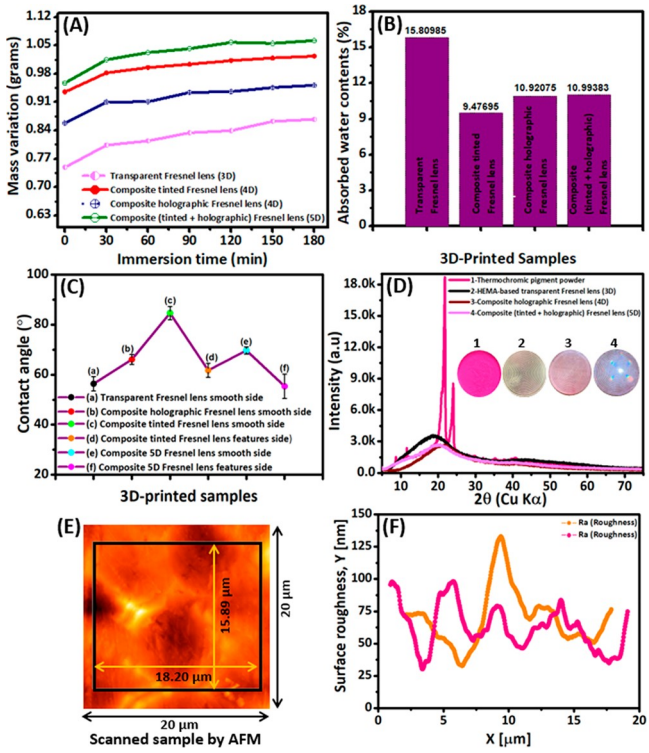

Figure 7. Various material characterizations of printed samples. (A) Mass increase of HEMA-based lens material over a 3 h immersion period. (B) Absorbed water content of various printed sample. (C) Contact angle measurements of printed samples on various surfaces (with and without features for Fresnel lenses). X-ray diffraction analysis of pigment powder and printed samples. (E,F) AFM image for surface quality evaluation (left) and surface roughness measurements by row (orange curve) and column (pink curve) approaches (right).

approach is viable since our lenses are stable and exhibit good repeatability (5 times repeated). The holographic effect of the 5D lens is still intact even at 36 °C and confirms the stable status of the hierarchal device. The simultaneously tunable temperature and optical response (fourth and fifth dimensions) of the 5D printed lens is demonstrated in Video S1 (Supporting Information).

The hydrogel material of the lens is known for its water retention, biocompatibility, and interesting hydration properties. Hence, we examined the printed hydrogel lenses for mass variation and water contents absorption while immersed in DI water for 3 h (Figure 7A,B). We dried the printed samples in an oven at 50 °C for 2 h to conduct the experiments. As is intrinsic to the hydrogel, the mass of all samples increased rapidly during the first 90 min of the immersion period,[49] and minimal changes occurred onward. The curve for the tinted Fresnel lens is smoother than that of others and might be attributed to the inclusion of pigment powder entangled in polymeric chains allowing the least mass variation. The water content absorption for all the lenses is presented in Figure 7A. As expected, the transparent Fresnel lens made of pristine HEMA hydrogel absorbed the maximum water content of around 16% (Figure 7B). Tinted and holographic lenses absorbed similar water content, indicating similar lens material modification. Tined lenses absorbed the least water content (~9.5%) due to pigment powders among polymeric chains, and the one-sided holographic pattern altered the lens surface wettability. Thus, the 5D lens also performed similarly due to the combined pigment powder and grating pattern inclusion, but the former modified the lens material slightly more.

In particular applications, our lenses could interact with fluid, such as integrating with soft contact lenses to detect glucose.[50] In addition, micro- and nanostructures can alter surface properties. Therefore, changes in surface characteristics need to be reported. The composite tinted lens recorded the highest contact angle (84.62° ± 2.59°) (Figure 7C). Each lens has two surfaces described as smooth and featured sides, without and with rings, respectively. The smooth surface offers minor surface roughness that leads to a higher contact angle. Also, the transparent lens is without material modifications and showed the lowest contact angle (56.38° ± 2.38°). The contact angles for all the lens surfaces are less than 90°, confirming the hydrophilic nature of the lens material (Figure 7C).[51] The

https://doi.org/10.1021/acsmaterialsau.2c00026
ACS Mater. Au 2022, 2, 602−613

holographic lens modified the lens surface by surface texturing and increased the contact angle from ∼56.38° to ∼66.10°, making the material more hydrophobic. Typically, laser technology is applied to generate surface texturing for specific applications.[52] Moreover, 5D printed lenses performed similarly, having a higher contact angle on the smoother side (69.62° ± 1.45°) than on the features side (55.36° ± 4.83°). The results suggest that surface wettability modification is more prominent due to the addition of pigment powders rather than from the embedded holographic patterns.

X-ray patterns for all the printed samples were obtained to examine crystallinity and new phase formation (Figure 7D). The powder material presented two peaks of 21.79° and 24.02° at 2θ, confirming the crystalline nature. However, the broad peak for the transparent lens of 18.58° at 2θ indicates that HEMA-based resin is amorphous in nature.[53] For the 5D printed Fresnel lens, no new phase formation was found, and the shift of the broad peak to 20.16° at 2θ might be due to curing processing. A similar change of the broad peak from 18.58° to 20.16° at 2θ is observed for the holographic lens. Finally, the printing process integrity without postprocessing for our printed lenses was evaluated by AFM characterization (Figure 7E,F). A selected region (represented by a black rectangular box) from a 20 × 20 μm^2 lens surface was chosen for surface roughness measurements (Figure 7E). The roughness measured by two different methods (row and column approaches) is presented in (Figure 7F). The average surface roughness values (R_a) measured by row (orange curve) and column (pink curve) approaches are ∼72 and ∼69 nm, respectively. Thus, these results confirm the high surface quality of our 3D printing process. Consequently, the surface quality of our lens (λ/4 to λ/10 quality) falls in the acceptable range of component surfaces fabricated with optimized printer parameters.[54]

4. CONCLUSIONS AND PROSPECTS

This work successfully manufactured 3D, 4D, and 5D Fresnel lenses with suitable optical properties. Remarkably, the fabrication of 5D printed Fresnel lens extends its functionalities as hierarchical device in optical systems, ensuring reduced cost and enhanced materials. 3D Fresnel lenses performed well to ensure lens characteristics of transmission and convergence of incoming light. The use of PVC film on the printer head resulted in improved average transmission reaching 91.4% for the transparent lens. Lenses also converged incident light with acceptable deviations from designed values despite wavelength-dependent focusing behavior. The pigment powder's addition to the transparent resin led to a fourth dimension of the Fresnel lens, and a stable thermal response (coloration and discoloration) in 25−36 °C range was observed. The response of the thermionic Fresnel lens was stable after five repetitions (fabrication and measurements), confirming the stability and durability of our lenses. In addition to thermal sensing, such lenses can be employed in selective wavelength filtering applications at room temperature. The photonic structures required to generate holographic sensors can be produced in several ways. Due to the optical properties being dependent on the spacing of fringes, micro- and nanoscale fabrications are often required. The fifth dimension of the Fresnel lens is evident from the digital images and SEM micrographs. The rainbow pattern generated could be easily combined with an image sensor providing a miniature spectrometer for mechanoluminescence sensing applications. AFM analysis revealed average roughness values of ∼72 and ∼69 nm with two approaches to confirm the quality of printed lenses. Although the lenses fabricated have suitable optical properties, further improvements are also possible. For instance, layer thickness of less than 25 μm can minimize the stairing effect and improve optical performance. Further progress in surface roughness is possible by using dip-coating with a similar resin material and then curing in a UV chamber. The fabricated lenses can be utilized in hydration sensing in future work.

■ ASSOCIATED CONTENT

Supporting Information

The Supporting Information is available free of charge at https://pubs.acs.org/doi/10.1021/acsmaterialsau.2c00026.

Fresnel lens design schematic; schematic illustration of resin-pigment powder mixture preparation (PDF)

Video of the Fresnel lens exhibiting focusing and rainbow holographic effect simultaneously (AVI)

■ AUTHOR INFORMATION

Corresponding Authors

Haider Butt − *Department of Mechanical Engineering, Khalifa University of Science and Technology, Abu Dhabi 127788, UAE; Advanced Digital & Additive Manufacturing Center, Khalifa University of Science and Technology, Abu Dhabi 127788, United Arab Emirates;* orcid.org/0000-0003-2434-9525; Email: haider.butt@ku.ac.ae

Murad Ali − *Department of Mechanical Engineering, Khalifa University of Science and Technology, Abu Dhabi 127788, UAE;* orcid.org/0000-0002-0939-7759; Email: murad.ali@ku.ac.ae

Author

Fahad Alam − *Department of Mechanical Engineering, Khalifa University of Science and Technology, Abu Dhabi 127788, UAE*

Complete contact information is available at: https://pubs.acs.org/10.1021/acsmaterialsau.2c00026

Notes

The authors declare no competing financial interest.

■ ACKNOWLEDGMENTS

The authors acknowledge Khalifa University of Science and Technology (KUST) for Award No. RCII-2019-003 and KU-KAIST Joint Research Center (Project code: 8474000220-KKJRC-2019-Health1) research funding in support of this research. We also acknowledge Sandooq Al Watan LLC and Aldar Properties for the research funding (SWARD Program − AWARD, Project code: 8434000391-EX2020-044).

■ REFERENCES

(1) Watson, J. K.; Taminger, K. M. B. A decision-support model for selecting additive manufacturing versus subtractive manufacturing based on energy consumption. *Journal of Cleaner Production.* **2018**, *176*, 1316−1322.

(2) Jonušauskas, L.; Mackevičiūtė, D.; Kontenis, G.; Purlys, V. Femtosecond lasers: the ultimate tool for high-precision 3D manufacturing. *Advanced Optical Technologies.* **2019**, *8*, 241−251.

(3) ISO/ASTM Standard 52900:2015. https://www.iso.org/standard/69669.html (accessed November 4, 2021).

(4) Bourell, D. L. Perspectives on Additive Manufacturing. *Annual Review of Materials Research.* **2016**, *46*, 1−18.

(5) Alam, F.; Elsherif, M.; AlQattan, B.; Salih, A.; Lee, S. M.; Yetisen, A. K.; Park, S.; Butt, H. 3D Printed Contact Lenses. *ACS Biomaterials Science & Engineering* **2021**, *7* (2), 794−803.
(6) Schmid, M.; Ludescher, D.; Giessen, H. Optical properties of photoresists for femtosecond 3D printing: refractive index, extinction, luminescence-dose dependence, aging, heat treatment and comparison between 1-photon and 2-photon exposure. *Optical Materials Express.* **2019**, *9*, 4564.
(7) Bertoncini, A.; Liberale, C. 3D printed waveguides based on photonic crystal fiber designs for complex fiber-end photonic devices. *Optica.* **2020**, *7*, 1487.
(8) Stübbe, O.; Huxol, A.; Villmer, F.-J. Applying fused layer modeling technologies to print embedded 3D optical waveguide structures for communication and sensor applications. In *3D Printed Optics and Additive Photonic Manufacturing*; von Freymann, G., Herkommer, A. M., Flury, M., Eds.; SPIE, 2018; p 16. DOI: 10.1117/12.2306910.
(9) Shrotri, A.; Beyer, M.; Stübbe, O. Manufacturing and analyzing of cost-efficient fresnel lenses using stereolithography. In *3D Printed Optics and Additive Photonic Manufacturing II*; von Freymann, G., Herkommer, A.M., Flury, M., Eds.; SPIE, 2020; p 25. DOI: 10.1117/12.2555367.
(10) Shrotri, A.; Beyer, M.; Schneider, D.; Stübbe, O. Manufacturing of lens array prototypes containing spherical and fresnel lenses for visible light communications using stereolithography apparatus. In *Laser 3D Manufacturing VIII*; Helvajian, H., Gu, B., Chen, H., Eds.; SPIE, 2021; p 40. DOI: 10.1117/12.2586907.
(11) Park, S. H.; Su, R.; Jeong, J.; Guo, S.-Z.; Qiu, K.; Joung, D.; Meng, F.; McAlpine, M. C. 3D Printed Polymer Photodetectors. *Adv. Mater.* **2018**, *30*, 1803980.
(12) Kong, Y. L.; Tamargo, I. A.; Kim, H.; Johnson, B. N.; Gupta, M. K.; Koh, T.-W.; Chin, H.-A.; Steingart, D. A.; Rand, B. P.; McAlpine, M. C. 3D Printed Quantum Dot Light-Emitting Diodes. *Nano Letters.* **2014**, *14*, 7017−7023.
(13) Pedrotti, H.; Pedrotti, F.; Bausch, L.; Schmitt, W. *Optik Fur Ingenieure: Grundlagen*; Springer: Berlin, 2008.
(14) Leutz, R.; Suzuki, A. *Lenses and Mirrors for Solar Energy, in: Nonimaging Fresnel Lenses*, 1st ed.; Springer-Verlag: Berlin, Heidelberg, 2001; pp 3−14. DOI: 10.1007/978-3-540-45290-4_2.
(15) Rajasekharan, R.; Butt, H.; Dai, Q.; Wilkinson, T. D.; Amaratunga, G. A. J. Can Nanotubes Make a Lens Array? *Adv. Mater.* **2012**, *24*, OP170−OP173.
(16) Aničin, B. A.; Babović, V. M.; Davidović, D. M. Fresnel lenses. *American Journal of Physics.* **1989**, *57*, 312−316.
(17) Egger, J. R. Use Of Fresnel Lenses In Optical Systems: Some Advantages And Limitations. In *Optical Systems in Engineering I*; Yoder, P.R., Jr., Ed.; SPIE, 1979; pp 63−69. DOI: 10.1117/12.957873.
(18) Ahmed, R.; Butt, H. Strain-Multiplex Metalens Array for Tunable Focusing and Imaging. *Advanced Science.* **2021**, *8*, 2003394.
(19) Zhang, C.; Cheng, G.; Edwards, P.; Zhou, M.-D.; Zheng, S.; Liu, Z. G-Fresnel smartphone spectrometer. *Lab on a Chip.* **2016**, *16*, 246−250.
(20) Min, K.-P.; Kim, J.; Song, K. D.; Kim, G.-W. A G-Fresnel Optical Device and Image Processing Based Miniature Spectrometer for Mechanoluminescence Sensor Applications. *Sensors.* **2019**, *19*, 3528.
(21) Li, D.; Sawhney, M.; Kurtz, R.; Solomon, L.; Collette, J. Impact of the Location of a Solar Cell in Relationship to the Focal Length of a Fresnel Lens on Power Production. *Energy Power* **2014**, *4*, 1−6.
(22) Huang, H.; Su, Y.; Gao, Y.; Riffat, S. Design analysis of a Fresnel lens concentrating PV cell. *International Journal of Low-Carbon Technologies.* **2011**, *6*, 165−170.
(23) Butt, H.; Rajesekharan, R.; Dai, Q.; Sarfraz, S.; Vasant Kumar, R.; Amaratunga, G. A. J.; Wilkinson, T. D. Cylindrical Fresnel lenses based on carbon nanotube forests. *Appl. Phys. Lett.* **2012**, *101*, 243116.
(24) Fresnel lenses for ultrasonic inspection. *J. Acoust. Soc. Am.* **1982**, *71*, 514−514.
(25) Klamkin, M. S. Mathematical modelling: die cutting for a fresnel lens. *Mathematical Modelling.* **1980**, *1*, 63−69.
(26) Molerón, M.; Serra-Garcia, M.; Daraio, C. Acoustic Fresnel lenses with extraordinary transmission. *Appl. Phys. Lett.* **2014**, *105*, 114109.
(27) Ali, U.; Karim, K. J. B. A.; Buang, N. A. A Review of the Properties and Applications of Poly (Methyl Methacrylate) (PMMA). *Polymer Reviews.* **2015**, *55*, 678−705.
(28) Kusko, M.; Avram, A.; Apostol, D. Design and fabrication of Fresnel lenses. In *2008 International Semiconductor Conference*; IEEE, 2008; pp 445−448. DOI: 10.1109/SMICND.2008.4703451.
(29) Loaldi, D.; Quagliotti, D.; Calaon, M.; Parenti, P.; Annoni, M.; Tosello, G. Manufacturing Signatures of Injection Molding and Injection Compression Molding for Micro-Structured Polymer Fresnel Lens Production. *Micromachines.* **2018**, *9*, 653.
(30) Zhang, C.; Li, Y.; Kang, W.; Liu, X.; Wang, Q. Current advances and future perspectives of additive manufacturing for functional polymeric materials and devices. *SusMater.* **2021**, *1*, 127−147.
(31) Stalder, A. F.; Melchior, T.; Müller, M.; Sage, D.; Blu, T.; Unser, M. Low-bond axisymmetric drop shape analysis for surface tension and contact angle measurements of sessile drops. *Colloids and Surfaces A: Physicochemical and Engineering Aspects.* **2010**, *364*, 72−81.
(32) Koncar, V. *Smart Textiles and Their Applications*; Woodhead Publishing, 2016. https://www.sciencedirect.com/book/9780081005743/smart-textiles-and-their-applications (accessed May 9, 2021).
(33) Stazi, F. Transparent Envelope. In *Advanced Building Envelope Components*; Elsevier, 2019; pp 1−53. DOI: 10.1016/B978-0-12-816921-6.00001-9.
(34) Zhou, C.; Heath, D. E.; Sharif, A. R. M.; Rayatpisheh, S.; Oh, B. H. L.; Rong, X.; Beuerman, R.; Chan-Park, M. B. High Water Content Hydrogel With Super High Refractive Index. *Macromolecular Bioscience.* **2013**, *13*, 1485−1491.
(35) Roberts, A. T.; Yang, J.; Reish, M. E.; Alabastri, A.; Halas, N. J.; Nordlander, P.; Everitt, H. O. Plasmonic nanoparticle-based epoxy photocuring: A deeper look. *Materials Today.* **2019**, *27*, 14−20.
(36) Emami, N.; Sjödahl, M.; Söderholm, K.-J. M. How filler properties, filler fraction, sample thickness and light source affect light attenuation in particulate filled resin composites. *Dental Materials.* **2005**, *21*, 721−730.
(37) MUSANJE, L.; DARVELL, B. Curing-light attenuation in filled-resin restorative materials. *Dental Materials.* **2006**, *22*, 804−817.
(38) Par, M.; Repusic, I.; Skenderovic, H.; Tarle, Z. Wavelength-dependent light transmittance in resin composites: practical implications for curing units with different emission spectra. *Clinical Oral Investigations.* **2019**, *23*, 4399−4409.
(39) Ali, M.; Alam, F.; Ahmed, I.; AlQattan, B.; Yetisen, A. K.; Butt, H. 3D printing of Fresnel lenses with wavelength selective tinted materials. *Additive Manufacturing.* **2021**, *47*, 102281.
(40) Alqurashi, T.; Montelongo, Y.; Penchev, P.; Yetisen, A. K.; Dimov, S.; Butt, H. Femtosecond laser ablation of transparent microphotonic devices and computer-generated holograms. *Nanoscale.* **2017**, *9*, 13808−13819.
(41) AlQattan, B.; Yetisen, A. K.; Butt, H. Direct Laser Writing of Nanophotonic Structures on Contact Lenses. *ACS Nano* **2018**, *12*, 5130−5140.
(42) Malinauskas, M.; Varapnickas, S.; Rekstyte, S.; Gailevicius, D.; Juodkazis, S.; Brasselet, E. Polarization effects in 3D femtosecond direct laser writing nanolithography. In *3D Printed Optics and Additive Photonic Manufacturing*; von Freymann, G., Herkommer, A. M., Flury, M., Eds.; SPIE, 2018; p 29. DOI: 10.1117/12.2306904.
(43) Smith, M.J.; Cope, E. The effects of temperature variation on single-lens-reflex digital camera calibration parameters. *International Archives of Remote Sensing and Spatial Information Sciences*, **2010**.
(44) Ali, M.; Alam, F.; Fah, Y.F.; Shiryayev, O.; Vahdati, N.; Butt, H. 4D printed thermochromic Fresnel lenses for sensing applications. *Composites, Part B* **2022**, *230*, 109514.
(45) León, K.; Mery, D.; Pedreschi, F.; León, J. Color measurement in L*a*b* units from RGB digital images. *Food Research International.* **2006**, *39*, 1084−1091.

(46) Gutub, A.; Al-Qahtani, A.; Tabakh, A. Triple-A: Secure RGB image steganography based on randomization. In *2009 IEEE/ACS International Conference on Computer Systems and Applications*; IEEE, 2009; pp 400−403. DOI: 10.1109/AICCSA.2009.5069356.
(47) Endres, F.; Hess, J.; Engelhard, N.; Sturm, J.; Cremers, D.; Burgard, W. An evaluation of the RGB-D SLAM system. In *2012 IEEE International Conference on Robotics and Automation*; IEEE, 2012; pp 1691−1696. DOI: 10.1109/ICRA.2012.6225199.
(48) Ahmad, M. F.; Alhady, S. S. N.; Rahiman, W.; Othman, W. A. F. W.; Zahir, A. A. M.. RGB Classification Determination with Different Light Intensity Using Pixy CMUcam5. In *Lecture Notes in Mechanical Engineering*; Springer, Singapore, 2018; pp 517−525. DOI: 10.1007/978-981-10-8788-2_46.
(49) Salih, A. E.; Elsherif, M.; Alam, F.; Yetisen, A. K.; Butt, H. Gold Nanocomposite Contact Lenses for Color Blindness Management. *ACS Nano* **2021**, *15*, 4870−4880.
(50) Elsherif, M.; Alam, F.; Salih, A. E.; AlQattan, B.; Yetisen, A. K.; Butt, H. Wearable Bifocal Contact Lens for Continual Glucose Monitoring Integrated with Smartphone Readers. *Small.* **2021**, *17*, 2102876.
(51) Read, M. L.; Morgan, P. B.; Kelly, J. M.; Maldonado-Codina, C. Dynamic Contact Angle Analysis of Silicone Hydrogel Contact Lenses. *Journal of Biomaterials Applications.* **2011**, *26*, 85−99.
(52) Sarbada, S.; Shin, Y. C. Superhydrophobic contoured surfaces created on metal and polymer using a femtosecond laser. *Appl. Surf. Sci.* **2017**, *405*, 465−475.
(53) Subramani, N. K. Revisiting Powder X-ray Diffraction Technique: A Powerful Tool to Characterize Polymers and their Composite Films. *Res. Rev.: J. Mater. Sci.* **2016**, *04*, 1−5.
(54) Blachowicz, T.; Ehrmann, G.; Ehrmann, A. Optical elements from 3D printed polymers. *E-Polymers.* **2021**, *21*, 549−565.

https://doi.org/10.1021/acsmaterialsau.2c00026
ACS Mater. Au 2022, 2, 602−613